International Journal of Nanomedicine

Dovepress
open access to scientific and medical research

Open Access Full Text Article

ORIGINAL RESEARCH

In vitro Evaluation of Paliperidone Palmitate Loaded Cubosomes Effective for Nasal-to-Brain Delivery

Laura Deruyver[1], Clément Rigaut[2], Alejandro Gomez-Perez[3], Pierre Lambert[2], Benoit Haut[2], Jonathan Goole[1]

[1]Laboratoire de Pharmacie Galénique et Biopharmacie, Faculté de pharmacie, Université libre de Bruxelles, Brussels, Belgium; [2]Transfers, Interfaces and Processes (TIPs), École Polytechnique de Bruxelles, Université libre de Bruxelles, Brussels, Belgium; [3]NanoMegas SRPL, Brussels, 1050, Belgium

Correspondence: Laura Deruyver, Boulevard du triomphe, CP207, accès 2, Campus Plaine, Bâtiment BC – 1B6 117, Brussels, 1050, Belgium, Tel +3226505221, Fax +3226505269, Email Laura.Deruyver@ulb.be

Introduction: This work aimed to develop chitosan-coated cubosomal nanoparticles intended for nose-to-brain delivery of paliperidone palmitate. They were compared with standard and cationic cubosomal nanoparticles. This comparison relies on numerous classical in vitro tests and powder deposition within a 3D-printed nasal cast.

Methods: Cubosomal nanoparticles were prepared by a Bottom-up method followed by a spray drying process. We evaluated their particle size, polydispersity index, zeta-potential, encapsulation efficiency, drug loading, mucoaffinity properties and morphology. The RPMI 2650 cell line was used to assess the cytotoxicity and cellular permeation. An in vitro deposition test within a nasal cast completed these measurements.

Results: The selected chitosan-coated cubosomal nanoparticles loaded with paliperidone palmitate had a size of 305.7 ± 22.54 nm, their polydispersity index was 0.166 ± 0.022 and their zeta potential was +42.4 ± 0.2 mV. This formulation had a drug loading of 70% and an encapsulation efficiency of 99.7 ± 0.1%. Its affinity with mucins was characterized by a ΔZP of 20.93 ± 0.31. Its apparent permeability coefficient thought the RPMI 2650 cell line was 3.00E-05 ± 0.24E-05 cm/s. After instillation in a 3D-printed nasal cast, the fraction of the injected powder deposited in the olfactory region reached 51.47 ± 9.30% in the right nostril and 41.20 ± 4.59% in the left nostril, respectively.

Conclusion: The chitosan coated cubosomal formulation seems to be the most promising formulation for nose-to-brain delivery. Indeed, it has a high mucoaffinity and a significantly higher apparent permeability coefficient than the two other formulations. Finally, it reaches well the olfactory region.

Keywords: cubosomes, nasal cast, charged nanoparticles, RPMI 2650 cell line, nose-to-brain delivery, nasal powder formulation, chitosan

Introduction

Paliperidone palmitate (PP) is a second-generation antipsychotic drug (SGAs)[1] used in the treatment of schizophrenia.[2] Antipsychotic drugs have several systemic side effects (sedation, weight gain, orthostatic hypotension or extrapyramidal effects[1,3]). Such adverse events are responsible for poor patient compliance, which usually leads to non-adherence to the therapeutic scheme. Indeed, a non-adherence of about 50% is estimated for schizophrenia.[4] Despite the reduction of the extrapyramidal effects brought by the SGAs, the increase in therapeutic adherence to the treatment of schizophrenia remains a considerable challenge.[1]

PP is also a poorly water-soluble drug,[3,5] commonly used via the intramuscular way (Xeplion® or Invega Sustenna®),[5,6] belonging to BCS class II.[7] Hence, it is necessary to increase its solubility and bioavailability by using formulation strategies or finding another administration way.

Received: 18 November 2022
Accepted: 1 February 2023
Published: 1 March 2023

Graphical Abstract

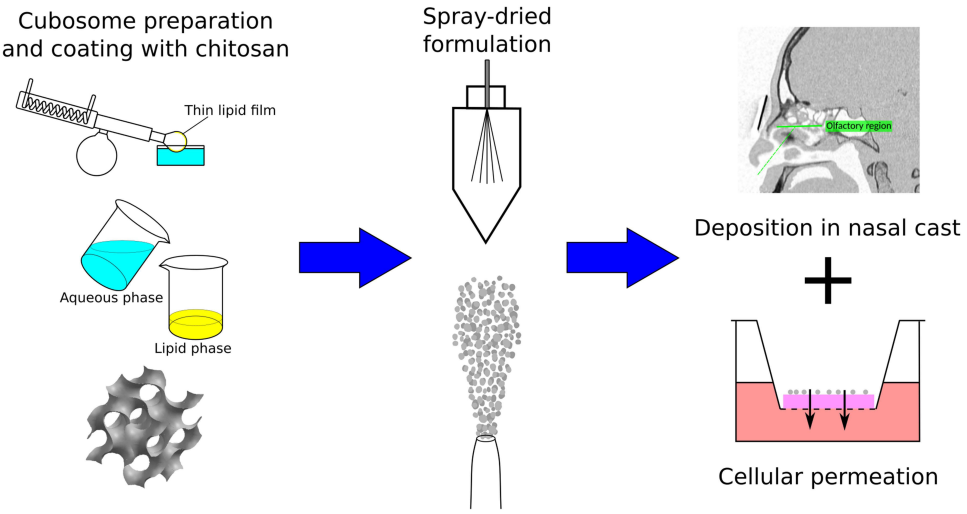

Nose-to-brain (N2B) delivery is a non-invasive route that aims to reach the brain by bypassing the blood-brain barrier (BBB).[1,8–13] From the intra-neuronal pathway, the drug enters the brain via the olfactory bulb (through the olfactory nerve) or the brain stem (through the trigeminal nerve),[12–14] which innerves the whole nasal cavity,[15] by axonal transport. The extra-neuronal pathway in olfactory epithelium[9,10,12,13] is based on para- or transcellular mechanisms.[16] After cellular uptake, the drug reaches the subarachnoid space and reaches the brain via the cerebrospinal fluid.[13] The olfactory route allows a faster passage than from the trigeminal[1,13] one. For instance, Ganger et al evaluated the duration of the transport between 1,5h to 6h and 17h to 56h through the olfactory and trigeminal nerves pathways, respectively.[17] Therefore, despite the relatively small area of the olfactory region (between 1.5 and 10% of the total area of the nasal cavity),[18] this work aims to develop N2B formulations of PP that, combined with the appropriate device, could reach significantly the olfactory region.[19,20]

An interesting new nanocarrier for PP could be the cubosomal nanoparticles (CNPs). These particles have a size range (between 10 and 500 nm[21,22]) adapted for N2B delivery. CNPs are non-lamellar liquid crystalline nanoparticles (NPs) that self-assemble by nanoprecipitation in an excess of water,[23,24] with two production methods: the so-called Top-down and Bottom-up methods.[21,25] The Bottom-up method has many advantages when compared with the Top-down method. This method allows working with lower energy inputs (thanks to the use of a hydrotrope) and, thus, encapsulate thermo-sensitives drugs to produce smaller and more stable NPs. Its simplicity makes it also more suitable for large scale production.[22–24] CNPs are composed of a bicontinuous lipid cubic phase with a single lipid bilayer that forms a continuous periodic membrane lattice structure with two interwoven water channels giving rise to the pores (5–10 nm.[21,22,25,26] These NPs present several advantages like biocompatibility, bioadhesivness and biodegradability. They also have a broader lipidic internal structure than liposomes, hence a higher drug loading. CNPs can also encapsulate hydrophilic, hydrophobic and amphiphile drugs; they are easy to produce and offer enzymatic protection.[21,24,27] Finally, their fundamental constituents: amphiphilic lipid (phytantriol, monoolein (MO) or glycerylmonooleate), steric stabilizers and water compounds[21,22,25,28] are all FDA-approved for human use. The interest for CNPs intended for N2B delivery has been recently reported. Indeed, Elsenosy et al developed cubo-gels with Duloxetine intended for N2B delivery. They demonstrated a brain bioavailability 1.96 times higher for their cubo-gel than the Duloxetine solution after an intranasal administration.[29] Eissa et al formulated a cubosomes-based in situ gel loaded with granisetron. They reported a maximum serum concentration of drugs (C_{max}) 1.90 times higher in rat brains with their cubosomal formulation (869.4 ng/mL) than with a Granisetron solution (457.2 ng/mL).[30]

The objective of this work is the development of dry chitosan-coated cubosomes and the comparison of their efficiency for N2B delivery with standard and cationic CNPs. Indeed, the literature describes many NPs coated with chitosan (e.g PLGA NPs,[31,32] liposomes,[20,33] nanostructured lipid carrier[34]) but no cubosomes. Dry formulations were used because their efficacity to reach the brain, in comparison with liquid formulations, was extensively reported.[19,35–37]

A reference formulation was inspired by Von Halling et al, which only used the MO to form the CNPs.[38] Their work was based on the research of Spicer et al about the formulation of dry powder precursors of liquid cubic crystalline NPs.[39] The second formulation was based on the addition of cholesterol (CHO) and a cationic lipid to produce positively charged CNPs. On one side, the cholesterol consolidates the lipid bilayer structure and reduces of thermal fluctuation of the CNPs.[26,40] Moreover, the charged lipid swells the internal structure of the CNPs and increases the water-channels diameters.[26,40] For this second formulation, 1,2-Dioleoyloxy-3-trimethylammonium propane chloride (DOTAP) was used as cationic lipid to allow a good affinity with the negatively charged mucins in the nasal mucosa due to electrostatic interactions.[1,41] Finally, for the third formulation, 1,2-Dioleoyl-sn-glycero-3-phosphoserine (DOPS) was used as anionic lipid. To generate positively charged CNPs to provide good interaction with the mucins, the anionic CNPs were coated with chitosan to finally obtain positively charged CNPs. Moreover, as reported in the literature, chitosan is an efficient permeation enhancer for N2B delivery.[42–46] In particular, it can open the tight junction (TJs) by dehydrating the epithelial cells and thus increase the paracellular transport in the olfactory epithelium.[10,45,46] This is a crucial factor in increasing the absorption of drugs. Also, the chitosan has mucoadhesive proprieties and can increase the residence time of the formulation in the olfactory region.[10,45,46] A recent study by Ahmad et al demonstrated the efficacity of PLGA-NPs coated with chitosan for brain targeting. Indeed, the C_{max} in the brain was 1.33 times higher for their PLGA-NPs coated with chitosan than for the drug suspension (5235.028 ± 5.00 and 3943.23 ± 5.77 ng/mL, respectively) after an intranasal administration in rats.[31] Thus, our work focused on developing a formulation using CNPs as an efficient carrier to encapsulate our lipophilic drug and chitosan to promote the permeation between the nasal epithelia. As described below, to cover the whole process of N2B delivery, we also used a nasal cast as a new tool for nasal in vitro assessment to map the pharmaceutic forms in the nasal cavities.[47]

Methods

Preparation and Characterization of the Formulations

Preparation of the Cubosomal Nanoparticles Liquid Formulations

The standard CNPs (SCNPs) were prepared using the Bottom-up method. Briefly, 5.33 mg/mL of MO (Danisco A/S, Denmark) were dissolved in ethanol and dispersed in an aqueous phase at a ratio of 1:3 v/v.[38] Dextran (Pharmacosmos, Denmark) and Kolliphor® P407 (BASF, Germany) (4.32 mg/mL and 173 µg/mL, respectively) were previously dissolved in MilliQ water. The resulting formulation was mixed for 15 minutes by moderate magnetic stirring.

For the preparation of the cationic and chitosan-coated cubosomal nanoparticles liquid formulations, several proportions of lipid mixtures were prepared by the thin lipid film hydration method to evaluate their influence on the physicochemical properties of the resulting cubosomes. Briefly, the lipid mixtures were composed of 70:25:5, 60:30:10, 50:35:15 and 40:40:20%MOL of MO, CHO (Sigma-Aldrich, USA) and charged lipids (DOTAP or DOPS, cationic and anionic lipids, respectively) (Lipoid GmbH, Germany). The lipids were introduced into a round-bottomed opaque flask and dissolved by a mixture of organic solvents (dichloromethane:methanol 50:50 v/v). Except for the blank formulations, the PP (Biochem Partner, China) was previously dissolved in the organic solvent-lipid mixture.

The organic solvents were removed within 20 minutes using a Rotavapor R-205 (Büchi Labortechnik, Flawil, Switzerland) at 60°C to produce a thin lipid film at the internal surface of the round-bottom flask. The pressure was set at 250 mmHg for 10 minutes and 150 mmHg for the next 10 minutes.

Finally, the Bottom-up method was used to generate the CNPs. This process relies on the lipid film dissolution by ethanol and, then, by the precipitation of the cubosomes by adding of an excess of an aqueous phase. In this work, Kolliphor® P407 (10% w/w of lipid mixture) was dissolved in MilliQ water to stabilize the colloidal system.

A further coating step of the anionic CNPs with chitosan followed this procedure to produce the chitosan-coated CNPs (ChCNPs) liquid formulation, this procedure was followed by a further step of coating the anionic CNPs with

chitosan low molecular weight (50–190 kDa, 75–85% deacetylated, Sigma-Aldrich, USA). A solution of 10% w/v of chitosan was prepared in 1% v/v acetic acid solution. Then, this solution was added drop by drop under vigorous magnetic stirring for 10 minutes in the previously formed anionic liquid formulation to obtain a final product with 0.1% w/v of chitosan. So, the anionic CNPs were positively charged thanks to the chitosan coating.

Preparation of the Powder Formulations Using Spray Drying

The spray drying was performed with a Mini Spray-Dryer B-290 (Büchi, Switzerland) equipped with a 0.7 mm diameter nozzle and a high-performance cyclone. The inlet temperature was 130°C; the spray gas flow was 357 L/h; the flow rate was fixed at 3 mL/min; the aspirator rate reached 100%. Ten milliliters of each liquid formulation were dried in triplicate.

After spray-drying, each powder formulation was dispersed in Milli-Q water at 1 mg/mL and briefly sonicated using a VCX 500 probe sonicator (Vibra-Cell; Sonics and Materials, Newton, CT, USA).

Then, the particle size (PS) (z-average, nm), the polydispersity index (PDI), and the zeta potential (ZP, mV) of the cubosomes were evaluated using dynamic light scattering (DLS) and electrophoretic mobility (Zetasizer® Nano ZS, Malvern Ltd., Malvern, England). Size measurements were performed with PS semi-micro disposable cuvettes (DTS0012) and zeta potential evaluation with disposable folded capillary cells (DTS1070). The temperature during the analysis was 25°C. All the experiments were repeated in triplicate and expressed as the mean ± SD (n=3). The pH of each reconstitution was determined using the pH-meter (VWR® pHenomenal® pH/mV/°C Meter, Bench, pH 1100L/1100LB).

Finally, the particle size distribution (PSD), the production yield and the percentage of the residual moisture of each powder formulation (SCNPs, CCNPs and ChCNPs) were compared without and with the use of 25% w/w of l-leucine (LL) (vegetal L-leucine, Sigma-Aldrich, USA). The PSD of the microparticles at the exit of the UDS device (Aptar Pharma, Le Vaudreuil, France) was measured via laser diffraction using a Spraytec apparatus in an open bench system with a 100 mm lens (Malvern® Instrument, Malvern, UK). The analysis parameters were: test duration of 300 ms, actuation distance of 7 cm and data acquisition rate of 2500 Hz. Size distribution was expressed in terms of first decile (Dv10), median diameter (Dv50), last decile (Dv90), and span value (experiments were done in triplicate).

The production yield (%) for the spray drying process was calculated as follows (Equation 1):

$$Yield\% = \frac{W_r}{W_i} X100 \tag{1}$$

where W_r is the mass of powder collected (mg) after drying, and W_i is the mass of components contained in the initial liquid formulation introduce in the spray drier (mg). The residual moisture (% w/w) of each powder formulation was evaluated by thermogravimetric analysis (TGA) using a TGA Q500 (TA Instruments, New Castle, Delaware, USA). The temperature cycle ranged between 35 and 150°C with a heat rate of 10°C/ min. The percentage of residual moisture was determined with TA Instrument Universal Analysis 2000 software by measuring the weight variation (% w/w).

Determination of Maximal Drug Loading Capacity and the Entrapment Efficiency

We added several amounts of pure PP to the SCNPs, CCNPs, and ChNPs liquid formulations to evaluate the maximal drug loading of each powder formulation. Equation 2 gives the maximal drug loading capacity (LC) of the cubosomes (%):

$$DL(\%) = \frac{W_{PP}}{W_{MO}} \tag{2}$$

where W_{PP} is the mass of PP (mg) and W_{MO} is the mass of MO (mg). Equation 3 gives the encapsulation efficiency (EE) of the cubosomes/:

$$EE(\%) = \frac{W_{PPi}}{W_{PPf}} \tag{3}$$

where W_{PPi} is the initial mass of PP introduced in the formulation (mg) and W_{PPf} is the mass of PP in the powder formulation after spray drying (mg).

We used an HPLC-UV method to quantify PP from the cubosomes. Five milligrams of each powder formulation were dissolved in a mixture of acetonitrile, ethanol and MilliQ water solution (45:45:10 v/v, respectively). The solutions were filtered through 0.45 µm filters (Sortorius®) and filled in 2 mL amber vials for HPLC analysis. As described by Manini et al, mobile phase A (100% v/v of acetonitrile) and mobile phase B (aqueous solution of trifluoroacetic acid at pH 2) were used at a ratio of 70/ 30 A/B (v/v). The flow rate was 1 mL/min for 20 min, and the wavelength was 278 nm. The retention time of PP was 8.0 min.[48] The pH of the mobile phase was evaluated by using a VWR® pHenomenal® pH/mV/°C Meter.

Powder X-Ray Diffraction

The powder formulations were evaluated by powder X-ray diffraction (PXRD) using an X-ray diffractometer (D8 Advance Eco Bruker). The measurement system was a one-dimensional silicon detector (LynxEye XE-T, Bruker) using Cu-K radiation (1.54 Å; 40 kV x 25 mA). Data were collected over the angular range of 1–40° 2θ, with a step size of 0.02°, a time step of 2 s and a variable divergence slit of 8 mm. The percentage of amorphous form was calculated as 100% minus the crystalline phase content in the powder, as determined using the surface area ratio method.

Characterization of the Morphology of the Nanoparticles

The cubosomal morphology of the optimized formulations was observed by transmission electron microscopy (TEM). 0.5 µL of a sample (1mg/mL in Milli-Q water) was placed onto the center of a commercial 3–5-layer graphene grid with a Lacey-C support (EMS). Then, a top grid allowed the droplet to expand and fill the nano-pockets while van der Waals forces joined the two grids to seal the system.

The system was placed in a single-tilt holder and introduced in a TECNAI G2 super-twin with a LaB6 filament, 30 µm CA2 aperture, operated at 200 kV. We worked in TEM mode using a Cheetah- MEDIPIX 3 direct detection camera (Amsterdam Scientific Instruments, Hollands) located in the 35 mm port of the microscope to obtain high-quality pictures using an extremely low electron flux (around 10^{-3} $e^{-}.Å^{-1}.s^{-1}$). An objective aperture of 30 µm optimized the contrast.

Scanning Electron Microscope Analysis

The morphology of the microparticles was studied by scanning electron microscope (SEM) analysis using a Hitachi SU8020 ultra-high-resolution microscope (Hitachi, Tokyo, Japan). The particles were coated with gold (35 mA for 4.5 min at 1 mbar under argon) before analysis. The images were processed using ImageJ software (National Institutes of Health, USA).

Plume Angle and Ejection Velocity

To evaluate the angle and the velocity of the plume from the UDS device (Aptar Pharma, Le Vaudreuil, France), a high-speed camera was used (IDT Motion Pro Y3, Integrated Design Tools, Pasadena, CA, USA with a Nikon AF micro-Nikkor 60 mm f/2.8 D lens, Nikon, Tokyo, Japan) (n=3). The parameters were: aperture of 16, acquisition time of 100 µs, and acquisition frequency of 3,000 Hz.

Mucoaffinity Test

A stock solution (400 µg/mL) was prepared by dissolving 20.0 mg of porcine-stomach mucins (type II, Sigma-Aldrich, USA) in 50.0 mL of MilliQ water. In addition, the stock solution was diluted with MilliQ water to provide four concentrations of mucins, namely 80, 160, 240, 320, and 400 µg/mL (S_{m1}, S_{m2}, S_{m3}, S_{m4}, and S_{m5}, respectively). The concentration of mucins was fixed to be in the detection range found when using the previously described method based on DLS. Each liquid formulation was reconstituted by mixing forty milligrams of the corresponding powder formulation in 20 mL of MilliQ water.

The evaluation method of the interaction between the mucin and the CNPs was based on the method of Wong et al.[49] One milliliter of each mucin solution (S_{m1}, S_{m2}, S_{m3}, S_{m4} and S_{m5}) and one milliliter of each reconstituted liquid formulations (SCNPs, CCNPs and ChCNPs) were mixed and incubated for 30 min in 37°C at 600 rpm.

The ZP of each solution was evaluated by DLS (Zetasizer® Nano ZS, Malvern Ltd., Malvern, England), along with the ΔZP to evaluate the mucoaffinity of each kind of CNPs (see Equation 4).

$$\Delta ZP = ZP_i - ZP_f \quad (4)$$

Where ZP_i is the initial ZP (mv) of the CNPs and ZP_f is the ZP (mv) of the CNPs after contact with mucin solution (S_{m5}). Each experiment was realized in triplicate and expressed by mean ± SD.

In vitro Cellular Study

RPMI2650 Cell Culture

The RPMI 2650 cell line is a common choice for an epithelial in vitro model for nasal permeation studies.[50–52] Indeed, this cell line produces mucus,[50] expresses TJs,[52,53] and grows in multilayer leading to appropriate transepithelial electrical resistance (TEER) values (between 75–150 Ωcm^2 and 90–180 Ωcm^2 for RPMI 2650 cell line and excised human nasal mucosa, respectively).[50,52,53] The RPMI 2650 cells (ECACC, Sigma-Aldrich, USA) were cultured in a 75 cm^2 polystyrene cell-culture flask under standard conditions in an incubator at 37 °C and 5% v/v of CO_2. The culture medium (MEM with phenol red, 10% heat-inactivated fetal bovine serum (FBS), 1% Pen/Strep solution, 1% L-glutamine and 1% NEAA, Thermo™ Fisher Scientific, USA) was changed every couple of days. The cells were detached when confluence reached about 80% by treating with trypsin-EDTA at 37°C. Then, the cells were seeded into a new 25 cm^2 polystyrene cell-culture flask at a 1:10 ratio.

As explained by Gonçalves et al, the RPMI 2650 cells were seeded on permeable Thincert® (TC-PTP, 0.4 µm, 4.52 cm^2, Thermo™ Fisher Scientific, USA) at a density of 1.5×10^5 cells/cm^2. The cells were cultured in a liquid-covered culture (LCC) for 8 days. The insert culture medium (MEM without phenol red, 10% heat-inactivated fetal bovine serum (FBS), 1% Pen/Strep solution, 1% L-glutamine and 1% NEAA) was changed every 2 or 3 days. After, the insert was lifted to the air-liquid interface (ALI) and cultured for 14 more days.[50] As reported by Wengst et al, the TEER value is significantly higher for the RPMI 2650 cells in ALI conditions compared to LCC conditions.[52] Their results, coupled with light microscopy analysis, demonstrate that, in LCC conditions, the cells grow in clusters with free spaces between them.[52] On the other hand, the ALI conditions increased the aerobic exposition, which correlates with epithelial barrier formation.[53]

The TEER was recorded using an epithelial Volt/Ohm meter EVOM2® (World Precision Instruments, Sarasota, USA). The value of the blank insert was subtracted from the raw data and normalized for the surface area (4.52 cm^2). For TEER routine evaluations, 2 mL of fresh insert culture medium were added to the apical side and 3 mL to the basal side. Cells were left for 30 min before measurements. A TEER value higher than 75 Ωcm^2 (mimicking the TEER of the human nasal mucosa[52]) was targeted to start the permeation study.

Alcian Blue Assay

The secretion of mucus on the surface of the mono/multilayer of RPMI 2650 cells was observed using Alcian blue (Thermo™ Fisher Scientific, USA) dye as described by Gonçalves et al.[50]

Images were acquired with an Olympus BX60 microscope (Olympus, Hamburg, Germany), equipped with a JVC tk-c1381 color video camera and an Olympus U-CMAD-2 C-Mount Adapter Ring, supported by the analySIS®docu image-processing software (Olympus).

The images were analyzed by ImageJ (V2.1.0, NIH) with the Color Inspector 3D V2.5 (Kai Uwe Barthel; Internationale MedieiInformatik, Berlin, Germany) plugin. To this end, each image was first transformed into 8-bit RGB. The average value over the whole picture of the blue component was then divided by the sum of the three channels (blue, red, and green). The resulting ratio allowed us to quantify the mucus produced by the cells.

Permeation Study

The study started after 22 days of culture to get the desired TEER value. A Krebs-Ringer buffer (KRB) was prepared to perform this permeation study. First, the cells were rinsed three times with KRB, and 1.0 mL was added to the apical side and 2.0 mL to the basolateral side. The plates were kept in an incubator (37°C, 5% CO_2) for 30 min. After, around 3 milligrams of each powder (pure PP, SCNPs, CCNPs, and ChCNPs) were deposed on the apical side. Each powder was introduced into three different inserts to perform the test in triplicate and diffused for three hours. The apparent

permeability coefficient (P_{app}) was calculated for each powder formulation by the following equation and expressed in cm/s[50,54] (Equation 5):

$$P_{app} = \frac{[C_b] \times V}{A \times [C_0] \times \Delta t} \quad (5)$$

where $[C_b]$ (µg/mL) is the concentration of PP in the basolateral compartment at the end of the experiment, $[C_b]$ (µg/mL) is the initial apical concentration of PP, V (mL) is the volume of the basolateral compartment, A is the surface area (cm^2) and $[C_b]$ is the duration of the experiment (s).

The Transport Enhancement Ratio (TER) of the formulation compared to the pure PP was calculated from the P_{app} values (Equation 6):

$$TER = \left(\frac{P_{app(formulation)}}{P_{app(PP)}}\right) \quad 6$$

where $P_{app(formulation)}$ corresponds to the Papp of SCNPs, CCNPS, and ChCNPs formulations and where $P_{app(PP)}$ corresponds to the P_{app} of PP.

The TEER was measured again 24 hours after the experiment to evaluate the integrity of the epithelium cells.

LDH Cytotoxicity Assay

An LDH assay was also carried out with the Cayman chemical kit (Item no 601,170) to measure the cytotoxicity of the three powder formulations. Cells were placed in a 96-well plate with a density of 50,000 cells/mL and allowed to settle for one hour. The cells were then treated with the formulations and analyzed following the kit manufacturer's instructions. The absorbance at 490 nm (A490) was measured and the percentage of cytotoxicity was expressed by the following equation:

$$Cytotoxicity(\%) = \left[\frac{(experimentalvalueA490) - (spontaneousreleaseA490)}{(maximumreleaseA490) - (spontaneousreleaseA490)}\right] \times 100 \quad (7)$$

Deposition Study in a Nasal Cast

Nasal Cast Conception

We used the 3D-printed nasal replica (called "nasal cast") described by Rigaut et al to assess the deposition profile of our formulations.[47] The selected patient has normal anatomy without any anatomical disorder. The nasal cast is a new in vitro test to evaluate drug deposition in a nasal cavity. The human nasal cavity is composed of tortuous and complex structures and varies between patients (e.g. sex, ethnicity, age or disease state). Thus, evaluating the olfactory targeting in vitro represents a pivotal element before the expensive in vivo test. Indeed, although nasal casts are not yet a regulatory test, a recent study by Williams et al validated this model as a suitable in vitro tool to assess in vivo deposition of a nasal product.[55]

Briefly, from the CT scan of a patient, the nasal cavities were separated from the body via the grey value: darker pixels are air, and lighter pixels are parts of the body. It resulted in a series of black-and-white images that could be assembled and smoothed to re-create the 3D model of the nasal cavity. Then, this model was segmented into five pieces to evaluate the spatial distribution of the spray in the cavity. The nasal cast was printed with a Form3 printer (Formlabs, Somerville, MA, USA) using Formlabs Clear resin, except for the nostrils, which were printed with Formlabs Flexible 80A resin to allow a better insertion of the devices. After printing, each part of the nasal cast was washed with isopropanol and UV-cured according to Formlabs guidelines.

Deposition Test

Each part of the nasal cast was coated with an artificial mucus based on a thermosensitive gel (liquid under 10°C and swells around 18°C) composed of 25% w/w of Poloxamer® 407 mixed into a simulated nasal electrolyte solution (SNES).[47,56] We introduced an exact amount of around 20 mg of powder into the device since the maximal dose for nasal delivery is 25 mg per nostril.[37,57] A previous study allowed us to determine the optimal parameters to target the olfactory

zone.[47] The insertion angle was fixed with a direct aim of the olfactory zone (sagittal angle of 39° on the right and 29° on the left, and coronal angle of 20° on the right and 5° on the left, both pointing inwards). There was no concomitant inspiratory flow, and the powder was injected with a UDS device (Aptar Pharma, Le Vaudreuil, France). The device was weighed before and after the injection to evaluate the administered dose. After instillation, we washed each part of the nasal cast with a mixture of acetonitrile, ethanol, and MilliQ water (45:45:10% v/v). Each recovery solvent was quantified by an HPLC-UV method to determine the percentage of powder in each part. Here, since the target is N2B delivery, the analysis was focused on the olfactory deposition (i.e. the deposition in the uppermost piece of the middle region).

Statistical Analysis

We used the one-way ANOVA test was used to demonstrate the significance of each factor for the comparison of CNPs with or without LL, the TER and the P_{app} comparison in the permeation study and for the comparison in the deposition test with the left and the right side. Student's *t*-test was used to study the difference in the mucoaffinity test. All statistical tests were performed by using GraphPad (Prism 9, San Diego, USA) and the difference between means was considered significant with a *p*-value lower than 0.05.

Results

Characterization of the Formulations

Spray-Dried Powder Properties

We compared the characteristics of the positively charged cubosomes (cationic CNPs (CCNPs) and ChCNPs) intended for N2B delivery to those of SCNPs that are created without CHO or a charged lipid to evaluate the potential efficacity.

The first step for the two charged blank CNPs (CCNPs and anionic CNPs) was to select the correct proportion of lipids to obtain stable and compatible NPs for N2B delivery. Indeed, it is necessary to formulate anionic CNPs as an intermediate step to coat them afterwards with chitosan by electrostatic interaction to obtain the ChCNPs. All test lipid mixtures gave NPs with a PS and a ZP suitable for N2 delivery. But only the mixture of 60:30:10%mol of MO, CHO, and an ionized lipid leads to a narrow PSD (i.e. PDI value lower than 0.3).

As mentioned previously, for N2B delivery, a positive surface charge of NPs increases their interaction and their affinity with the negatively-charged mucins of the nasal mucosa.[1,10] So, the selected anionic CNPs were coated with chitosan to obtain a final positive charged CNPs called ChCNPs. The summary of the selected blank CNPs with their characteristics is shown in Table 1.

The two positively charged CNPs were characterized by a positive ZP (+60.1 ± 1.2 and +34.4 ± 1.2 mV for CCNPs and ChCNPs respectively) while the SCNPs were characterized by a negative ZP. Since a ZP higher than +20 mV or lower than −20mV is known to be favorable for long-term stability,[10] the two positively charged CNPs are more stable than the SCNPs.

Table 1 Particles Size (PS) (Nm), Polydispersity Index (PDI) Value and Zetapotential (ZP) (mV) of Selected Blank Standard Cubosomal Nanoparticles (SCNPS), Cationic Cubosomal Nanoparticles (CCNPS), Anionic Cubosomal Nanoparticle (Anionic CNPS), and Chitosan-Coated Cubosomal Nanoparticles (ChCNPS). Results are Expressed by Mean ± SD

Blank Formulation	PS (nm)	PDI	ZP (mV)
SCNPs	153.7 ± 6.2	0.353 ± 0.014	−9.0 ± 0.7
CCNPs	142.7 ± 1.3	0.242 ± 0.004	+60.1 ± 1.2
Anionic CNPs	109.9 ± 0.7	0.297 ± 0.022	−66.7 ± 4.5
ChCNPs	249.8 ± 15.9	0.234 ± 0.050	+34.4 ± 1.2

NPs with a PS lower than 200 nm can diffuse through olfactory neurons.[42,58,59] All blank CNPs were characterized by a particle size lower than 200 nm except for the ChCNPs (see Table 1), which had a PS of 249.8 ± 15.9 nm. However, the benefits of chitosan as a permeation enhancer should offset this slight deviation in size.[10,60,61] Indeed, Raj et al demonstrated a higher dopamine content in the brain after an intranasal administration of Pramipexole loaded in chitosan NPs (despite a PS of 292 ± 8.80 nm) versus a solution of the same drug (97.38 ± 3.91 ng/g tissue and 81.61 ± 4.44 ng/g tissue respectively).[62] Finally, in our study, all blank CNPs demonstrated a narrow particle size distribution which a PDI value lower than 0.3,[63] except the SCNPs with a slightly higher value of 0.353 ± 0.014, which should not have any consequence on their suitability.

During the spray drying process, a sticky powder in the cyclone was observed. Indeed, a high residual moisture content promotes the formation of liquid bridges between particles which solidify after drying to generate agglomerates.[64–67] Moreover, a high residual moisture content reduces the glass transition temperature (T_g). Therefore, when the experimental temperature is higher than the Tg of the material, it becomes sticky (rubbery state) and adheres to the cyclone.[65,66] Adding LL in a range between 10–20% w/w increases the yield of production and the flowability of the particles, and reduces the residual moisture and the caking effect.[64,68–71] As LL is a hydrophobic amino acid, it will dry faster than the other formulation compounds, which could create a shell around the drug.[65] Indeed, droplet drying is characterized by two distinct steps: the constant-rate period and the falling-rate period. The materials characterized by a high Peclet number, such as LL, tend to concentrate onto the droplet surface as evaporation is faster than their diffusion.[65] Preliminary studies were performed to determinate the optimal LL content to improve the powder PSD (data not shown), to increase the spray-drying yield and to decrease the residual moisture content of the dry powders. To evaluate the influence of LL, its percentage was fixed at 25% w/w in each formulation (Table 2).

As shown in Table 2, the yield was similar, regardless of the presence of LL (higher than 70% w/w). Although, in the absence of LL, the residual moisture content was higher than 2% w/w, while the addition of the amino acid allowed us to obtain a lower percentage. Therefore, the yield was slightly overestimated for the powders that were not based on LL.

These results illustrated the anti-hygroscopic effect of LL[64,66,67,69,72] and could explain the decrease of powder agglomerates. Indeed, the LL increased the moisture resistance of the spray-dried particles by its surface enrichment. This, in turn, reduced the thickness of the liquid on the surface of the particles and reduced the liquid bridges between them.[67,73] It allowed both improving the deagglomeration and the flowability of the powder.

The deagglomeration effect is illustrated by the Dv50 value of each powder formulation measured at the exit of the UDS device. Indeed, all powder formulations containing LL were characterized by a Dv50 smaller than the powder without LL (14.49 ± 0.63 µm, 14.34 ± 0.82 µm, and 12.65 ± 0.37 µm for SCNPs-LL, CCNPs-LL, and ChCNPs-LL, respectively and 78.42 ± 14.61 µm, 61.02 ± 9.30 µm and 43.76 ± 12.04 µm for SCNPs, CCNPs and ChCNPs, respectively).

Table 2 Size Distribution Was Expressed in Terms of First Decile (Dv10), Median Diameter (Dv50), Last Decile (Dv90), and Span Value. The Yield (%) and Residual Moisture Content (%) Were Expressed for Standard Cubosomal Nanoparticles (SCNPs), Cationic Cubosomal Nanoparticles (CCNPs), and Chitosan-Coated Cubosomal Nanoparticles (ChCNPs) Blank Formulation with or Without l-Leucine (LL). Results are Expressed by Mean ± SD

Blank Formulations	Dv_{10} (µm)	Dv_{50} (µm)	Dv_{90} (µm)	Span	% Yield	% Moisture
SCNPs	31.89 ± 7.24	78.42 ± 14.61	119.14 ± 17.52	1.13 ± 0.08	70.73	2.209
SCNPs-LL	11.25 ± 0.88	14.49 ± 0.63	52.37 ± 3.45	2.83 ± 0.11	77.57	1.838
CCNPs	18.44 ± 2.86	61.02 ± 9.30	103.62 ± 14.50	1.40 ± 0.05	73.26	2.254
CCNPs-LL	11.91 ± 0.28	14.34 ± 0.82	38.55 ± 10.03	1.84 ± 0.59	77.98	1.843
ChCNPs	12.68 ± 1.81	43.76 ± 12.04	77.95 ± 15.06	1.51 ± 0.15	74.39	2.167
ChCNPs-LL	8.65 ± 3.61	12.65 ± 0.37	23.33 ± 10.47	1.66 ± 1.27	75.86	1.710

The Dv50 of our LL-containing powders ranged between 13 and 20 µm. Such diameters are known to promote olfactory zone impaction and thus the passage to the brain.[74–76]

Determination of the Maximal Drug Loading Capacity and the Encapsulation Efficiency

We studied the maximal LC (Equation 2) of each CNPs and checked their EE (Equation 3) by introducing several quantities of PP (fixed percentage shown in Table 3) and analyzing the effect on the PSD of the CNPs. The maximal LC selected is 10%, 5%, and 70% for the SCNPs, CCNPs, and ChCNPs, respectively, because these LCs gave the lowest PDI value for each CNPs formulation and thus, guaranteed a narrow PSD with a PS suitable for the N2B delivery (Table 3). The CCNPs and SCNPs formulations provided the lowest LC, 5% and 10% w/w, respectively, while the LC of the ChCNPs formulation reached 70% w/w.

The PP is a strongly basic drug (pKa_1 8.2 and pKa_2 2.6),[77] and the pH of liquid pre-formulations was around 4.5 for each formulation, leading to positively-charged PP. So, electrostatic repulsion between the positively charged PP and the positively charged lipid during the production process could explain the lowest LC obtained for the CCNPs. In contrast, there was an attraction between the drug and the negatively-charged CNPs during the production process (SCNPs and ChCNPs before chitosan coating). For SCNPs and ChCNPs, the difference between the LC (10% and 70% w/w, respectively) could be explained by the cubosomal structure of ChCNPs: CHO stiffens the bilayer, and the anionic lipid (DOPS) electrostatically swells the structure, which allowed increasing the LC.[40,78,79]

Table 3 Loading Capacity (LC) (%), Particles Size (PS) (Nm), Polydispersity Index (PDI), pH, and Encapsulation Efficiency (EE) (%) of Each Selected Standard Cubosomal Nanoparticles (SCNPS), Cationic Cubosomal Nanoparticles (CCNPS), and Chitosan-Coated Cubosomal Nanoparticles (ChCNPS). And Zeta-Potential (ZP) (mV) of Each Selected CNPs Formulation. Results are Expressed by Mean ± SD

Loaded Formulation	LC (%)	PS (nm)	PDI	pH of the Reconstituted Powder	EE (%)	ZP (mV)
SCNPs	10	141.7 ± 4.4	0.334 ± 0.071	4.574	98.3 ± 1.8	+14.2 ± 0.3
	20	162.6 ± 5.5	0.393 ± 0.035	4.326	99.4 ± 0.1	–
	30	219.5 ± 9.8	0.475 ± 0.096	4.295	95.4 ± 0.1	–
	40	176.4 ± 5.9	0.410 ± 0.072	4.496	97.3 ± 0.4	–
CCNPs	2.5	112.1 ± 1.3	0.289 ± 0.035	4.397	81.4 ± 0.9	–
	5	116.5 ± 2.5	0.253 ± 0.027	4.463	98.0 ± 0.4	+66.4 ± 1.2
	7.5	161.2 ± 14.7	0.406 ± 0.055	4.345	98.6 ± 0.0	–
	10	139.7 ± 4.5	0.412 ± 0.061	4.261	98.0 ± 0.3	–
ChCNPs	60	238.2 ± 18.9	0.214 ± 0.049	4.356	99.3 ± 0.2	–
	70	305.7 ± 22.54	0.166 ± 0.022	4.475	99.7 ± 0.1	+42.4 ± 0.2
	80	387.7 ± 28.9	0.478± 0.049	4.476	96.2 ± 0.1	–
	90	285.9 ± 9.6	0.378 ± 0.074	4.364	97.3 ± 0.2	–

Finally, the EE of each selected formulation is higher than 95% (98.3 ± 1.8%, 98.0 ± 0.4% and 99.7 ± 0.1% for SCNPs, CCNPs, and ChCNPs, respectively) and they are stable, given their ZP value (Table 3), which should be ideally either above +20 mV or below −20 mV.[10]

Powder X-Ray Diffraction

To evaluate the crystallinity and the stability of our powder formulations, the PXRD profiles of pure PP, dextran and CNPs were studied (Figure 1). The CNPs formulations were mostly amorphous (Figure 1A) due to the presence of dextran (Figure 1B).

In each powder formulation, the peaks of LL are at 6° and 19° 2θ [80] and 30° and 32.5° 2θ. The main peaks of crystallinity of PP at 2° and 7.5° 2θ were observed for the SCNPs and ChCNPs powders. For the CCNPs powder, only the typical peak at 2° 2θ was observed. It could be the consequence of the low concentration of PP in the CCNPs powder formulation.

In Figure 1A, the PXRD profile of chitosan extracted to the ICDD database[81] (vertical red lines) suggested that the two peaks at 20.3° and 21.4° 2θ for the ChCNPs formulation correspond to the chitosan coating. Indeed, these two peaks are missing in the two other formulations which did not contain chitosan.

Characterization of the Morphology of the Cubosomes

The morphology of each CNPs was performed with TEM analysis. The SCNPs were nearly spherical with polyangular irregular shapes (Figure 2A). In previous studies, Elsenosy et al, as well as Nasr et al, already observed that loaded cubosomes usually lose their cubic shape.[29,82] In contrast, although they were also loaded with PP, the CCNPs and ChCNPs preserved their cubic structure (Figure 2B and C). The addition of cholesterol in both formulations may explain this observation. Indeed, before the TEM analysis, the powder was reconstituted by sonication in Milli Q water. This

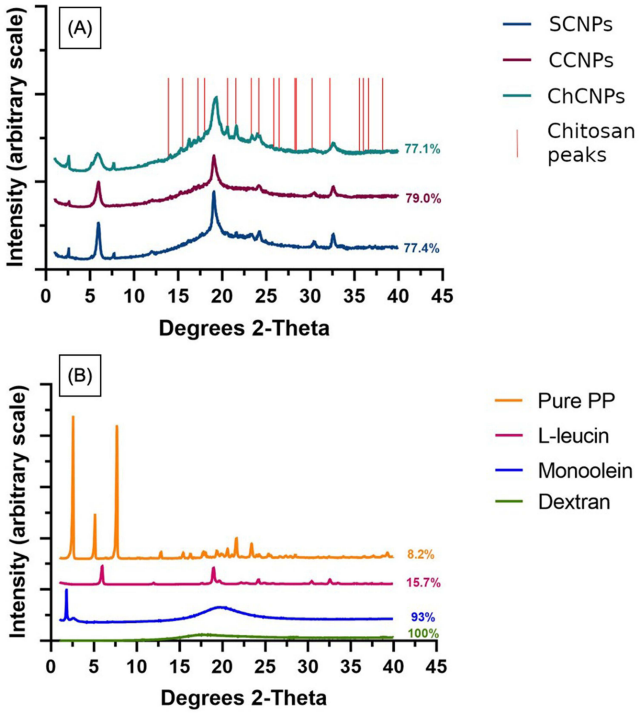

Figure 1 (**A**) XRPD profile of the three powder formulations: standard cubosomal nanoparticles (SCNPs), cationic cubosomal nanoparticles (CCNPs), and chitosan-coated cubosomal nanoparticles (ChCNPs), the vertical red lines correspond to the peaks of chitosan extracted to ICDD database[81]; (**B**) XRPD profile of pure paliperidone palmitate (PP), l-leucine, monoolein and, dextran. The percentage of amorphous form was indicated on the right of the curve.

Notes: Data from Gates–Rector S, Blanton T. The powder diffraction file: a quality materials characterization database. Powder Diffr. 2019;34(4):352–360. doi:10.1017/S0885715619000812.[81]

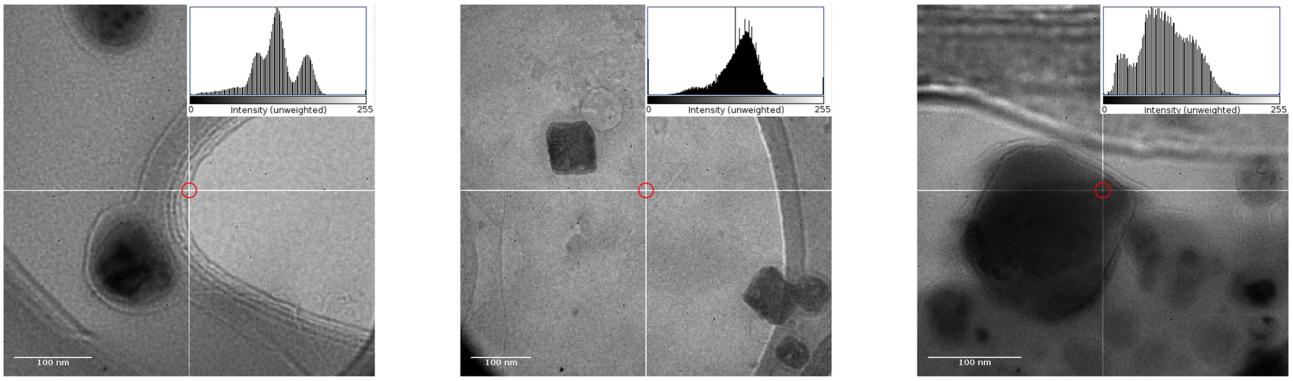

Figure 2 TEM image of (**A**) standard cubosomal nanoparticles (SCNPs), (**B**) cationic cubosomal nanoparticles (CCNPs), and (**C**) chitosan-coated cubosomal nanoparticles (ChCNPs). It corresponds to the final product loading with paliperidone palmitate.

process is known to generate heat stress that may change the cubosomal shape. We may assume that cholesterol reduced thermal fluctuation and consolidated the lipid bilayer structure responsible for the cubosomal structure.[26,40]

Surprisingly, the mean diameter observed by TEM was lower than by DLS. Eissa et al[30] and Nasr et al[82] made similar observations. In contrast to the DLS measurements which were performed after the dispersion of the powder in water, TEM analysis was done in a vacuum on the dry powders themselves. Such difference may explain our observations.

Scanning Electron Microscope Analysis

The SEM showed that using the LL as an excipient for spray drying process induces corrugated particles[65,83] (see Figure 3). Indeed, LL has a high Péclet number which causes a surface enrichment during the spray drying process, which results in these corrugated particles.[65] By creating a shell around the dried particles, LL reduced the water vapor escaping during the spray drying process, inducing an increase vapor pressure. At the end of the process, the vapor pressure was decreased and yielded corrugated particles.[73]

For dry powder inhalers (DPIs), a high deposition performance seems to correlate with the corrugated surface of the powder. It is principally due to the reduction of agglomeration and the reduction of the interparticular forces.[65]

Plume Angle and Ejection Velocity

All powder formulations were characterized by a plume angle lower than 30° when instilled from the UDS (20.13 ± 2.65°, 18.87 ± 1.66°, and 17.73 ± 0.65° for the SCNPs, CCNPs, and ChCNPs, respectively). These values follow those previously observed using similar UDS and caffeine as a drug model (16.8° ± 2.4°).[47] A narrow plume angle seems to decrease the impaction in the nasal valve, increasing the postnasal-valve deposition.[84–86] For powder formulation, the plume angle is only affected by the administration device.[47] Indeed, the main factors influencing the plume of liquid sprays (viscosity, surface tension, and actuation force)[87] are fixed for dry sprays since the propellant gas is always the same (air in our case), and the actuation force set by the design of the device.

The ejection velocity of each powder formulation (49.53 ± 7.58 m/s, 42.40 ± 2.31 m/s, and 47.28 ± 4.33 m/s for the SCNPs, CCNPs and ChCNPs, respectively) was at least twice higher than the one observed with a liquid formulation (around 15 m/s[88]). A high ejection velocity reduces the influence of air friction on the microparticles.[47] Therefore, for a given patient and a given administration side, the particle trajectories are only influenced by the device orientation.[47]

Mucoaffinity Test

In addition to proteins such as albumin or immunoglobulins, the nasal mucus contains 95% water, less than 1% lipids, 2% mucin, and 1% of other salts.[17,58,89] Due to sialic and sulfonic acids, mucins are responsible for negative charges in the nasal mucosa.[17,90–92] The use of positively charged NPs increases the affinity, the residence time in the nasal mucosa and the bioavailability of the drug.[10]

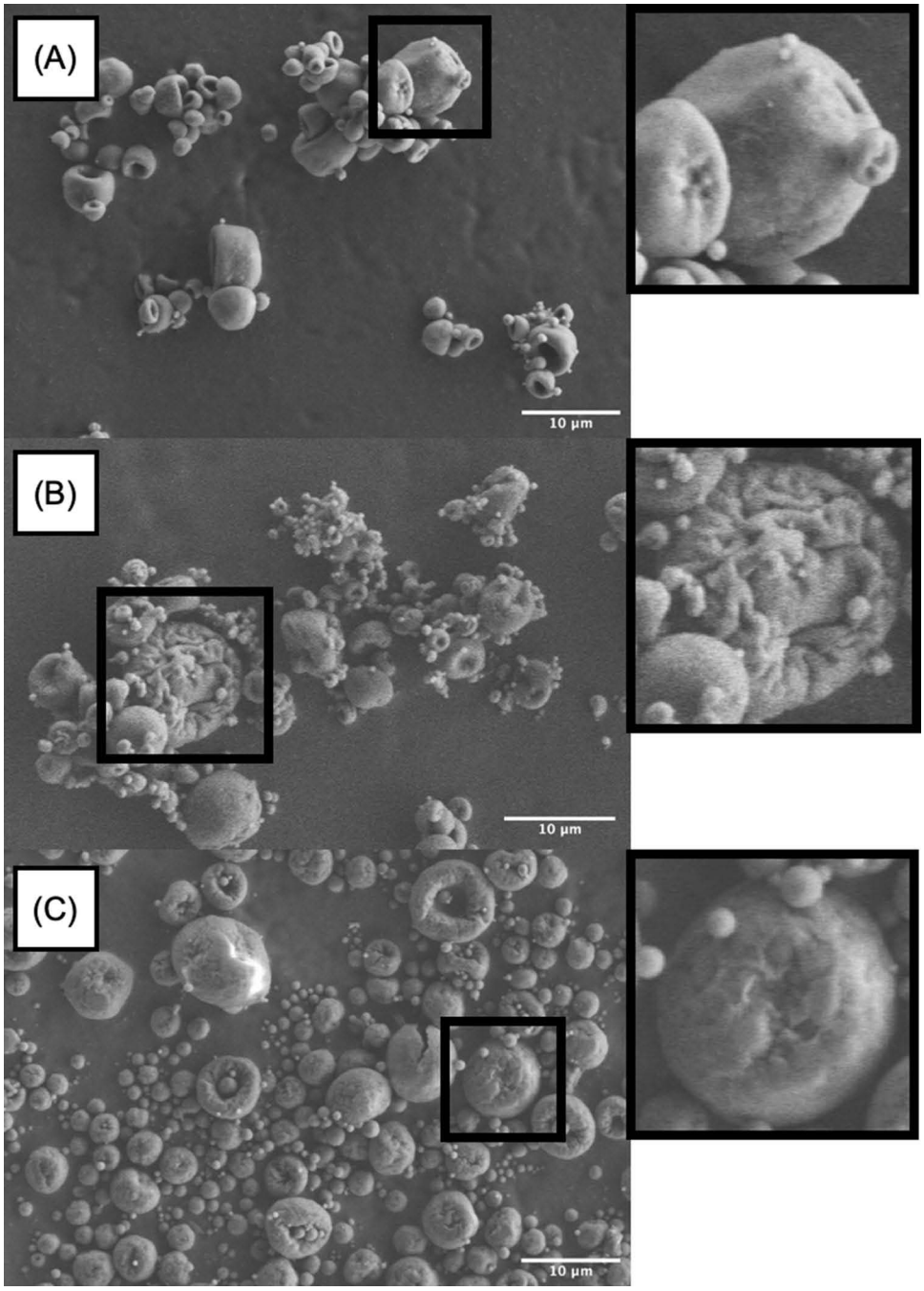

Figure 3 SEM images of corrugated microparticles. (**A**) standard cubosomal nanoparticles powder formulation with l-leucin, (**B**) cationic cubosomal nanoparticles powder formulation with l-leucin, and (**C**) chitosan-coated cubosomal nanoparticles powder formulation with l-leucin.

As mentioned previously, the ZP of each formulation upon contact with solutions of mucin at different concentrations was evaluated. A sharp decrease of the ZP from 14.2 ± 0.3 to −18.8 ± 4.6 mV was observed when the SCNPs were placed upon contact with S_{m1}, in comparison with the initial solution. Then, the ZP becomes independent of the mucin concentration and equal to the ZP of the mucin solution (see Figure 4A). Such results confirmed that there was no electrostatic interaction between the SCNPs and the mucins. That seemed to be correlated with the poor positive charge of these NPs. As illustrated in Figure 4A, the ZP of the CCNPs and the ChCNPs decreased with an increase in the mucin concentration. Moreover, the ΔZP was twice higher for the CCNPs than the ChCNPs (Figure 4B).

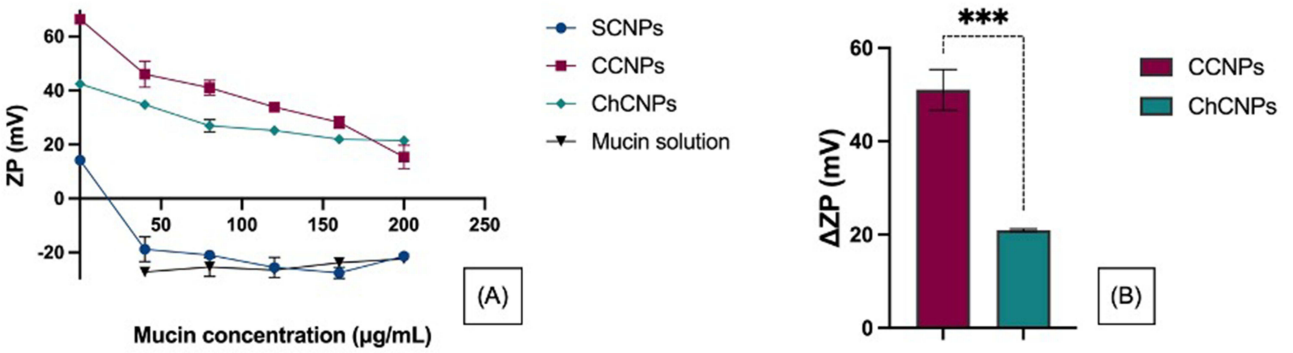

Figure 4 (**A**) Influence of the mucin concentration on the zetapotential (ZP) of standard cubosomal nanoparticles (SCNPs), cationic cubosomal nanoparticles (CCNPs), and chitosan-coated cubosomal nanoparticles (ChCNPs); (**B**) Comparison of the $^{+}\Delta ZP$ of the CCNPs and ChCNPs. The results are expressed by mean ± SD. A statistical Student's *t*-test concluded a significant difference between the ΔZP of the two formulations ***p-value < 0.001). $^{+}\Delta ZP$ corresponds to the difference between the initial ZP (mv) of the cubosomal nanoparticles (ZP_i) and the ZP of the cubosomal nanoparticles after contact with mucin solution (ZP_f). $\Delta ZP = ZP_i - ZP_f$.

As previously described, the reconstituted liquid formulation had a pH of 4.574, 4.463 and 4.475 for SCNPs, CCNPs and ChCNPs, respectively. At this pH, the chitosan was positively charged due to the protonation of the amino group which generated an electrostatic interaction with the sulphate and the carboxyl group of the mucin.[90,93,94] The strong mucin electrostatic interaction with the CCNPs could easily be explained by the highly positively charged surface due to the incorporation of the cationic lipid. The molar concentration of DOTAP was higher than the one of the chitosan (6.2E-2 mole/g and 7.0E-4 mole/g of formulation for CCNPs and ChCNPs, respectively). Thus, there were more amino groups to interact with the mucins. This observation of increasing interaction with increasing amino groups is also supported by Mazzarino et al. In a recent study, they correlated a rise in the electrostatic interaction between the mucins and chitosan with the increase in the molar mass of the chitosan.[94]

In vitro Cellular Study

Permeation Study

In our study, the main aim was to compare the mucoaffinity between SCNPs and cationic formulations (CCNPs and ChCNPs) and the ability of the ChCNPs to open the TJs. Indeed, the human nasal mucosa is characterized by goblet cells responsible for mucus secretion and by ciliated epithelium with TJs.[50,52,95,96] Therefore, the RPMI 2650 cells were cultured in ALI condition from day 8 to day 22 to reach a TEER above 75 Ωcm^2 in order to mimic the TEER of nasal mucosa as mainly reported.[50,52]

As previously described by Gonçalves et al, the Alcian blue assay was used to characterize mucin production by RPMI 2650 cells.[50] An increase in the RGB_b ratio was observed after the 11th day (0.3290 ± 0.007 and 0.4002 ± 0.020 for the day 6 and the day 11, respectively) (Figure 5). It correlated with the beginning of the culture in ALI condition (on the 8th day) and illustrated the start of mucin production. When the cells started to produce mucus, the drug permeation study was performed as soon as the TEER value was higher than 75 Ωcm.[2]

All the CNPs formulations were characterized by a significative higher P_{app} than pure PP, except for the SCNPs formulation (Figure 6A). Such data confirmed the interest in improving the mucoaffinity of the cubosomes with a cationic lipid (CCNPs) or adding a permeation enhancer such as chitosan to open the TJs (ChCNPs). The P_{app} coefficient was increased from 2.57E-08 ± 3.025E-08 cm/s for the pure PP to 2.23E-06 ± 0.46E-06 cm/s for the SCNPs, to 1.72E-05 ± 0.21E-05 cm/s for the CCNPs and finally to 3.00E-05 ± 0.24E-05 cm/s for the ChCNPs. The ChCNPs were characterized by a significantly higher TER (86.86 ± 17.97, 671.25 ± 79.82 and 1168.38 ± 93.90 for SCNPs, CCNPs and ChCNPs, respectively) due to their mucoaffinity and ability to open the TJs (Figure 6B).

Several results are highlighted in the literature. First, it is well-known that the cationic NPs have a higher cellular uptake than the negatively charged NPs in commonly used cell lines.[97–100] However, in ex vivo studies, the results are more nuanced. Recent research conducted by Clementino et al demonstrated a higher initial (after 1 hour) sustained transport of their drug with their chitosan-coated NPs (their only positively charged formulation) across excised nasal

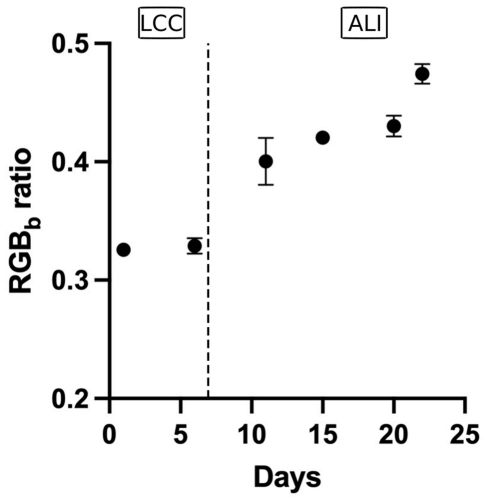

Figure 5 $^{+}RGB_b$ as a function of the culture duration (mean ± SD, n=3). LCC = liquid-covered culture and ALI = air-liquid interface cultivation. $^{+}RGB_b$ (Red-Green-Blue) ratio corresponding to the average value over the whole picture of the blue component was then divided by the sum of the three channels.

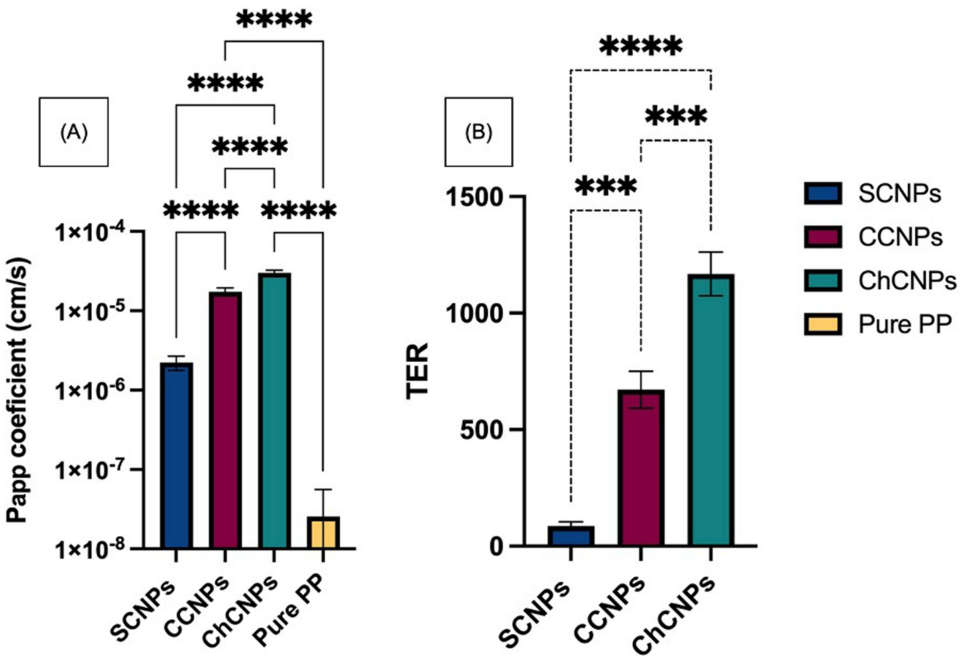

Figure 6 (**A**) Apparent permeability coefficient through the RPMI 2650 cell line of standard cubosomal nanoparticles (SCNPs), cationic cubosomal nanoparticles (CCNPs), chitosan-coated cubosomal nanoparticles (ChCNPs), and of the pure paliperidone palmitate (PP). The y-axis is expressed in log 10. Each comparison has a p-value < 0.0001 ****Except between pure PP and SCNPs (no significant). (**B**) The Transport Enhancement Ratio (TER) of each formulation compared to the pure PP. ****p-value < 0.0001 and ***p-value < 0.001. The results are expressed by mean ± SD and are realized in triplicate. The comparison was realized by a one-way ANOVA statistical test.

mucosa of rabbits (3-fold and 18-fold lower for their two other negatively charged NPs).[100] Indeed, their chitosan-coated NPs are drug vehicles that firmly anchor in the nasal mucosa. It improves drug absorption by lower colloidal stability upon mucus contact and by the specific biodegradation carried out by enzymes.[100]

On the other hand, another recent study compared the permeation of negatively and positively charged NPs through the olfactory mucosa.[101] Albarki et al concluded in better permeation with the negatively charged NPs.[101] They explained such results as their study was performed for one hour, although other studies were conducted for a longer period of time.[101] The work of Albarki et al contradicts Clementino et. al, but they only studied the effect of the charge while

Clementino et al added chitosan, a permeation enhancer.[100] Moreover, the difference between the work of Albarki et al and previous studies could be due not only to the timescale of the experiments but also to the difference between cancerous and normal cells.[31]

LDH Cytotoxicity Assay

The TEER value was unchanged before and 24h after the beginning of the permeation test. It confirmed the integrity of the cell barrier. In addition, the LDH cytotoxicity assay demonstrated the safety of the formulations except for the CCNPs. Indeed, we observed an increase in the percentage of cytotoxicity correlated with the positive surface charge (18.4 ± 1.3, 53.7 ± 3.2, and 32.2 ± 0.8% of cytotoxicity for SCNPs, CCNPs and ChCNPs respectively). However, the literature mainly described the cytotoxicity effect of the positively charged NPs in tumoral cells.[31,102,103] We observed a decrease in the percentage of cytotoxicity between the CCNPs and ChCNPs. It is probably due to the reduction of the positive surface charge. On the other hand, chitosan is extensively studied, and its cytotoxicity effect is negligible in normal cells.[31,103] For instance, a recent in vivo safety study by Abas et al concluded no significant irritation either for the placebo or for the drug-loaded chitosan formulations.[33]

Deposition Study in a Nasal Cast

We compared the percentage of olfactory deposition in the right and in the left cavities of the nasal cast for each CNPs dry formulation (Figure 7). Coherently with our previous study on the same cast,[47] the percentage of olfactory deposition in the right side (52.91 ± 8.85%) was always larger than in the left side (35.80 ± 8.46%). The size of the olfactory region (11.4 cm^2 and 10.5 cm^2 for the right and the left side, respectively[47]) could explain this difference. However, an ear, nose and throat (ENT) specialist of Erasme Hospital identified the CT scan of our patient as a non-pathologic nasal cavity; a perfect symmetry of the nasal cavity being inexistent in the population. Interestingly, Figure 7 also shows that the deposition in the olfactory region was statistically similar regardless of the CNPs powder. Therefore, it seemed that the anatomy of the nasal cavity had the most influence on the deposition than the physical properties of the powder with this combination system (UDS device with our powder formulation). Indeed, all formulations had a similar Dv50, plume angle, and ejection velocity. As previously described, the plume angle and the ejection velocity depend only on the device. The UDS device generates a narrow plume angle with a high ejection velocity and a direct aim at the olfactory region.

Figure 8 gives information on the general profile of deposition on both sides. A one-way ANOVA test concluded a significant difference between the left and the right side of the nose, the olfactory region, and the middle turbinates (p-value = 0.0106, < 0.0001, and <0.0001 respectively).

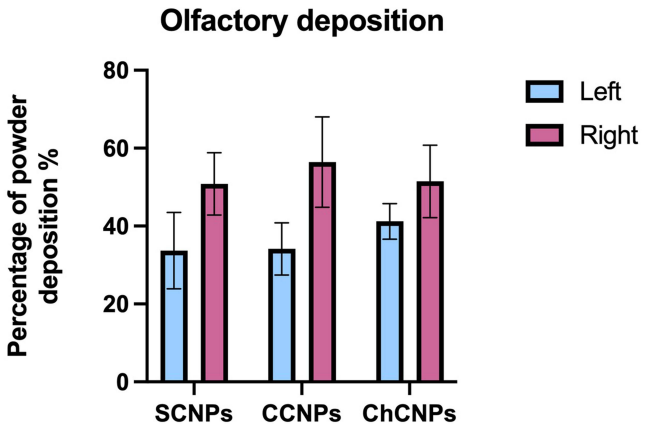

Figure 7 Percentage of the powder deposited on the olfactory region for the standard cubosomal nanoparticles (SCNPs), cationic cubosomal nanoparticles (CCNPs), and chitosan-coated cubosomal nanoparticles (ChCNPs) formulations in the left side and in the right side. Results are expressed by mean ± SD.

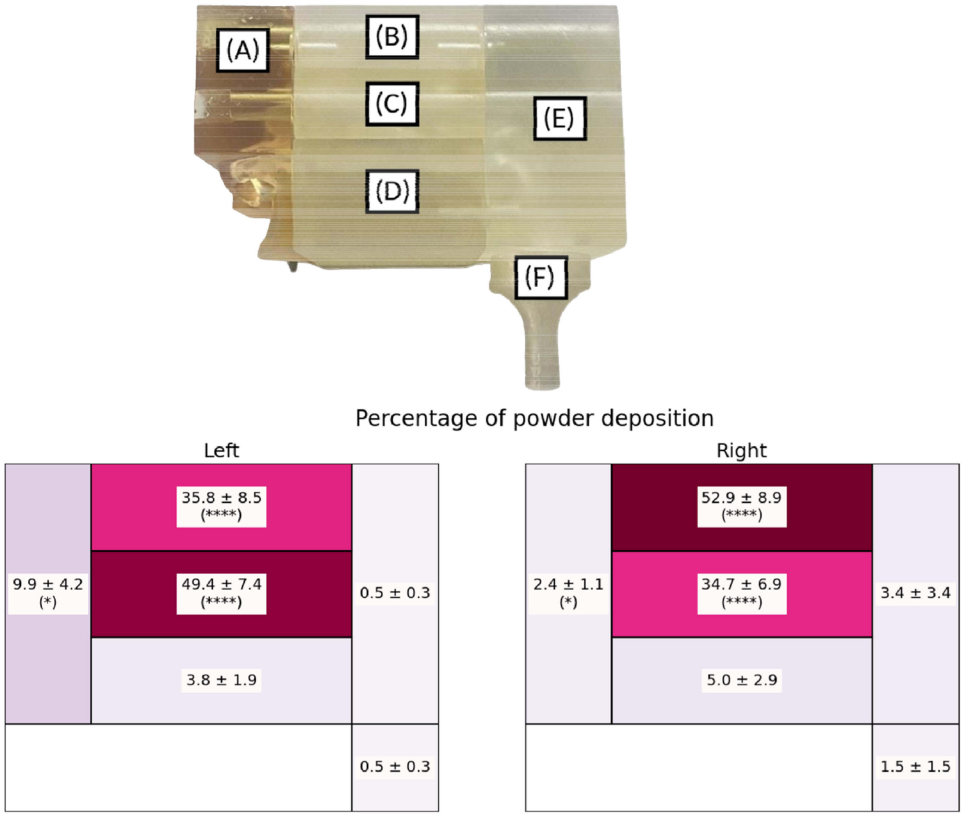

Figure 8 Percentage of powder deposition in (**A**) nostril, (**B**) olfactory, (**C**) middle turbinates, (**D**) lower turbinates, (**E**) nasopharynx, and (**F**) post-nasal fraction in left and right side for combined formulations. Results are expressed by mean ± SD. A one-way ANOVA statistical test was realized to compare the powder deposition in the right and in left side in each part of the nasal cast. *Indicate a p-value <0.05 and ****Indicate a p-value < 0.0001.

A higher deposition in the middle turbinates part than in the olfactory region was observed in the left nostril (49.4 ± 7.36 and 35.8 ± 8.46% for the middle turbinates region and the olfactory region respectively). Another interesting observation was the low deposition in the nasopharynx and post-nasal parts.

This deposition profile seemed to be favorable for brain targeting. Indeed, besides the olfactory nerves, another pathway to reach the brain after nasal instillation is through the trigeminal nerve which innerves the whole nasal cavity, except the post-nasal fraction.[15]

Finally, our results correlated with the results of Williams et al, which validated their in vitro deposition with an in vivo study. Indeed, in their work, the majority of the powder was also found in the middle turbinates and the olfactory region in the nasal cast (about 40 and 35% for the middle turbinates and the olfactory region, respectively) and in the in vivo study (about 35 and 38% for the turbinates and the olfactory region, respectively).[55]

Conclusion

The existing literature vastly underlines the potential of CNPs for hydrophobic drug administration and the advantageous nasal deposition of dry powder sprays compared to liquid sprays. So, our work focused on a dry cubosome formulation of PP intended for N2B delivery. To this end, we successfully developed three: one following the usual cubosome preparation method, and two innovative ones, incorporating cationic lipid or chitosan. After their comparison, we selected the ChCNPs. Indeed, the properties of these CNPs are adapted for N2B delivery in terms of PS, PDI and ZP. Finally, their P_{app} thought the RPMI 2650 cell line was 3.00E-05 ± 0.24E-05 cm/s. Since the pure PP has a P_{app} of 2.57E-08 ± 3.02E-08 cm/s, the formulation enables a 1000-fold increase in cell-diffusion efficiency. Furthermore, the powder deposition study in a 3D-printing nasal cast revealed that the powder mainly deposited in the olfactory region (51.47 ± 9.30% of olfactory deposition in the right side and 41.20 ± 4.59% of olfactory deposition in the left side, respectively).

This good result arises from the combination of an appropriate Dv50 and an adapted administration device intended for N2B delivery via the production of a narrow plume angle and a high ejection velocity. These results in the nasal cast are encouraging, given the promising in vivo – in vitro correlation obtained by Williams et al.[55] However, an in vivo study remains necessary considering the discrepancies between cell lines and ex vivo permeation studies but also to determine if nasal irritation is low enough given the in vitro cytotoxicity results. Such studies will be the subject of a future paper. But, despite the absence of an in vivo study, the CNPs seem to be a great choice of nanocarrier for nasal administration. In the addition, the use of nasal cast as a new tool for in vitro evaluation for N2B formulation could be beneficial to make progress in nasal powder formulation studies.

Abbreviations

API, active pharmaceutical ingredient; ALI, air-liquid interface cultivation; BBB, blood-brain-barrier; CHO, cholesterol; CCNPs, cationic cubosomal nanoparticles; ChCNPs, chitosan-coated cubosomal nanoparticles; CNPs, cubosomal nanoparticles; DLS, dynamic light scattering; DPIs, drug powder inhalers; EE, encapsulation efficiency; ENT, the ear, nose and throat FBS, fetal bovine serum; KRB, Krebs-ringer buffer; LC, loading capacity; LCC, liquid-covered cultivation; LDH, lactate dehydrogenase; LL, l-leucin; MO, monoolein; N2B, nose-to-brain; NPs, nanoparticles; Papp, apparent permeation coefficient; PDI, polydispersity index; PP, paliperidone palmitate; PS, particles size; PSD, particle size distribution; PXRD, powder X-ray diffraction; SCNPs, standard cubosomal nanoparticles; SD, standard deviation; SEM, scanning electron microscopy; SGAs, second generation antipsychotic drugs; SNES, simulated nasal electrolyte solution; Tg, glass transition; TGA, thermogravimetric analysis; TEM, transmission electron microscopy; TER, transport enhancement ratio; TEER, transepithelial electrical resistance; TJs, thigh junction; UDS, Uni-dose system; ZP, zeta potential.

Ethics Statement

The studies involving human participants were reviewed and approved by the Ethics Committee of Erasme Hospital – ULB (P2022/075). The Ethics Committee waived the requirement of written informed consent for participation.

Acknowledgments

The authors thank Tiriana Segato (4Mat, ULB, Brussels, Belgium) for her help during the PXRD investigation. The authors also thank Yoann Paint (MateriaNova, Mons, Belgium) for the SEM analysis. The authors thank Marc Vander Ghinst (Hôpital de Bruxelles (HUB), CUB Hôpital Erasme, department of Ear, Nose and Throat, and Cervico-facial surgery, Brussels, Belgium) for his expertise in nasal cavities.

AptarGroup (Aptar, Le Vaudreuil, France) kindly provided the unidirectional UDS devices.

This research was supported by the equipment of the Micro-mili platform.

Disclosure

The authors declare that this study received equipment from AptarGroup. The equipment providers were not involved in the study design, collection, analysis, interpretation of data, the writing of this article or the decision to submit it for publication. The authors report no other conflicts of interest in this work.

References

1. Tan MSA, Parekh HS, Pandey P, Siskind DJ, Falconer JR. Nose-to-brain delivery of antipsychotics using nanotechnology: a review. *Expert Opin Drug Deliv*. 2020;17(6):839–853. doi:10.1080/17425247.2020.1762563
2. McCutcheon RA, Reis Marques T, Howes OD. Schizophrenia - an overview. *JAMA Psychiatry*. 2020;77(2):201–210. doi:10.1001/jamapsychiatry.2019.3360
3. Citrome L. Paliperidone palmitate - review of the efficacy, safety and cost of a new second-generation depot antipsychotic medication. *Int J Clin Pract*. 2009;64(2):216–239. doi:10.1111/j.1742-1241.2009.02240.x
4. Acosta FJ. Medication adherence in schizophrenia. *World J Psychiatry*. 2012;2(5):74. doi:10.5498/wjp.v2.i5.74
5. Chue P, Chue J. A review of paliperidone palmitate. *Expert Rev Neurother*. 2012;12(12):1383–1397. doi:10.1586/ern.12.137
6. Zingale E, Bonaccorso A, Carbone C, Musumeci T, Pignatello R. Drug nanocrystals: focus on brain delivery from therapeutic to diagnostic applications. *Pharmaceutics*. 2022;14(4):691. doi:10.3390/pharmaceutics14040691

7. Maniyar AJ, Patel GM, Shelat PK, Lalwani AN. Development and characterization of thermosensitive intranasal gel containing paliperidone loaded microspheres. *J Young Pharm*. 2016;8(4):368–377. doi:10.5530/jyp.2016.4.12
8. Emad NA, Ahmed B, Alhalmi A, Alzobaidi N, Al-Kubati SS. Recent progress in nanocarriers for direct nose to brain drug delivery. *J Drug Deliv Sci Technol*. 2021;64:102642. doi:10.1016/j.jddst.2021.102642
9. Hussein NR, Omer HK, Elhissi AMA, Ahmed W. Advances in nasal drug delivery systems. In: Waqar Ahmed DA, Phoenix MJ editors. *Advances in Medical and Surgical Engineering*. Elsevier; 2020:279–311. doi:10.1016/B978-0-12-819712-7.00015-2
10. Deruyver L, Rigaut C, Lambert P, Haut B, Goole J. The importance of pre-formulation studies and of 3D-printed nasal casts in the success of a pharmaceutical product intended for nose-to-brain delivery. *Adv Drug Deliv Rev*. 2021;113826. doi:10.1016/j.addr.2021.113826
11. Wang Z, Xiong G, Tsang WC, Schätzlein AG, Uchegbu IF. Nose-to-brain delivery. *J Pharmacol Exp Ther*. 2019;370(3):593–601. doi:10.1124/jpet.119.258152
12. Illum L. Is nose-to-brain transport of drugs in man a reality? *J Pharm Pharmacol*. 2010;56(1):3–17. doi:10.1211/0022357022539
13. Selvaraj K, Gowthamarajan K, Karri VVSR. Nose to brain transport pathways an overview: potential of nanostructured lipid carriers in nose to brain targeting. *Artif Cells Nanomed Biotechnol*. 2017;46(8):1–8. doi:10.1080/21691401.2017.1420073
14. Thorne RG, Emory CR, Ala TA, Frey WH. Quantitative analysis of the olfactory pathway for drug delivery to the brain. *Brain Res*. 1995;692(1–2):278–282.
15. Thorne RG, Pronk GJ, Padmanabhan V, Frey WH. Delivery of insulin-like growth factor-I to the rat brain and spinal cord along olfactory and trigeminal pathways following intranasal administration. *Neuroscience*. 2004;127(2):481–496. doi:10.1016/j.neuroscience.2004.05.029
16. Illum L. Transport of drugs from the nasal cavity to the central nervous system. *Eur J Pharm Sci*. 2000;11(1):1–18.
17. Gänger S, Schindowski K. Tailoring formulations for intranasal nose-to-brain delivery: a review on architecture, physico-chemical characteristics and mucociliary clearance of the nasal olfactory mucosa. *Pharmaceutics*. 2018;10(3):116. doi:10.3390/pharmaceutics10030116
18. Bourganis V, Kammona O, Alexopoulos A, Kiparissides C. Recent advances in carrier mediated nose-to-brain delivery of pharmaceutics. *Eur J Pharm Biopharm*. 2018;128:337–362. doi:10.1016/j.ejpb.2018.05.009
19. Nižić Nodilo L, Ugrina I, Špoljarić D, et al. A dry powder platform for nose-to-brain delivery of dexamethasone: formulation development and nasal deposition studies. *Pharmaceutics*. 2021;13(6):795. doi:10.3390/pharmaceutics13060795
20. Salade L, Wauthoz N, Vermeersch M, Amighi K, Goole J. Chitosan-coated liposome dry-powder formulations loaded with ghrelin for nose-to-brain delivery. *Eur J Pharm Biopharm*. 2018;129:257–266. doi:10.1016/j.ejpb.2018.06.011
21. Chaudhary K, Sharma D. Cubosomes: a Potential Drug Delivery System. *Asian J Pharm Res Dev*. 2021;9(5):93–101. doi:10.22270/ajprd.v9i5.981
22. Thadanki M, Kumari PS, Prabha KS. Overview of cubosomes: a nano particle. *Int J Res Pharm Chem*. 2011;1(3):535–541.
23. Spicer PT, Hayden KL, Lynch ML, Ofori-Boateng A, Burns JL. Novel process for producing cubic liquid crystalline nanoparticles (cubosomes). *Langmuir*. 2001;17(19):5748–5756. doi:10.1021/la010161w
24. Karami Z, Hamidi M. Cubosomes: remarkable drug delivery potential. *Drug Discov Today*. 2016;21(5):789–801. doi:10.1016/j.drudis.2016.01.004
25. Yaghmur A, Tran BV, Moghimi SM. Non-lamellar liquid crystalline nanocarriers for thymoquinone encapsulation. *Molecules*. 2020;25(1):1–14. doi:10.3390/molecules25010016
26. Barriga HMG, Holme MN, Stevens MM. Cubosomes: the next generation of smart lipid nanoparticles? *Angew Chemie Int Ed*. 2019;58(10):2958–2978. doi:10.1002/anie.201804067
27. Chountoulesi M, Perinelli DR, Pippa N, et al. Physicochemical, morphological and thermal evaluation of lyotropic lipidic liquid crystalline nanoparticles: the effect of stimuli-responsive polymeric stabilizer. *Colloids Surfaces a Physicochem Eng Asp*. 2020;595:124678. doi:10.1016/j.colsurfa.2020.124678
28. Chong JYT, Mulet X, Waddington LJ, Boyd BJ, Drummond CJ. Steric stabilisation of self-assembled cubic lyotropic liquid crystalline nanoparticles: high throughput evaluation of triblock polyethylene oxide-polypropylene oxide-polyethylene oxide copolymers. *Soft Matter*. 2011;7(10):4768–4777. doi:10.1039/c1sm05181d
29. Elsenosy FM, Abdelbary GA, Elshafeey AH, Elsayed I, Fares AR. Brain targeting of duloxetine hcl via intranasal delivery of loaded cubosomal gel: in vitro characterization, ex vivo permeation, and in vivo biodistribution studies. *Int J Nanomedicine*. 2020;15:9517–9537. doi:10.2147/IJN.S277352
30. Eissa EM, Elkomy MH, Eid HM, et al. Intranasal delivery of granisetron to the brain via nanostructured cubosomes-based in situ gel for improved management of chemotherapy-induced emesis. *Pharmaceutics*. 2022;14:7. doi:10.3390/pharmaceutics14071374
31. Ahmad S, Khan I, Pandit J, et al. Brain targeted delivery of carmustine using chitosan coated nanoparticles via nasal route for glioblastoma treatment. *Int J Biol Macromol*. 2022;221:435–445. doi:10.1016/j.ijbiomac.2022.08.210
32. Fong SS, Foo YY, Saw WS, et al. Chitosan-coated-PLGA nanoparticles enhance the antitumor and antimigration activity of stattic – a STAT3 dimerization blocker. *Int J Nanomedicine*. 2022;17:137–150. doi:10.2147/IJN.S337093
33. Abbas H, El Sayed NS, Youssef NAHA, et al. Novel luteolin-loaded chitosan decorated nanoparticles for brain-targeting delivery in a sporadic alzheimer's disease mouse model: focus on antioxidant, anti-inflammatory, and amyloidogenic pathways. *Pharmaceutics*. 2022;14(5):1–26. doi:10.3390/pharmaceutics14051003
34. Yasir M, Zafar A, Noorulla KM, et al. Nose to brain delivery of donepezil through surface modified NLCs: formulation development, optimization, and brain targeting study. *J Drug Deliv Sci Technol*. 2022;75:103631. doi:10.1016/j.jddst.2022.103631
35. Calmet H, Inthavong K, Eguzkitza B, Lehmkuhl O, Houzeaux G, Vázquez M. Nasal sprayed particle deposition in a human nasal cavity under different inhalation conditions. *PLoS One*. 2019;14(9):e0221330–e0221330. doi:10.1371/journal.pone.0221330
36. Warnken ZN, Smyth HDCC, Davis DA, Weitman S, Kuhn JG, Williams RO. Personalized medicine in nasal delivery: the use of patient-specific administration parameters to improve nasal drug targeting using 3D-printed nasal replica casts. *Mol Pharm*. 2018;15(4):1392–1402. doi:10.1021/acs.molpharmaceut.7b00702
37. Maaz A, Blagbrough IS, De Bank PA. In vitro evaluation of nasal aerosol depositions: an insight for direct nose to brain drug delivery. *Pharmaceutics*. 2021;13(7):1079. doi:10.3390/pharmaceutics13071079
38. von Halling Laier C, Gibson B, van de Weert M, et al. Spray dried cubosomes with ovalbumin and Quil-A as a nanoparticulate dry powder vaccine formulation. *Int J Pharm*. 2018;550(1–2):35–44. doi:10.1016/j.ijpharm.2018.08.036

39. Spicer PT, Small WB, Lynch ML, Burns JL. Dry powder precursors of cubic liquid crystalline nanoparticles (cubosomes). *J Nanoparticle Res*. 2002;4(4):297–311. doi:10.1023/A:
40. Tyler AII, Barriga HMG, Parsons ES, et al. Electrostatic swelling of bicontinuous cubic lipid phases. *Soft Matter*. 2015;11(16):3279–3286. doi:10.1039/c5sm00311c
41. Cone RA. Barrier properties of mucus. *Adv Drug Deliv Rev*. 2009;61(2):75–85. doi:10.1016/j.addr.2008.09.008
42. Bhattamisra SK, Shak AT, Xi LW, et al. Nose to brain delivery of rotigotine loaded chitosan nanoparticles in human SH-SY5Y neuroblastoma cells and animal model of Parkinson's disease. *Int J Pharm*. 2020;579. doi:10.1016/j.ijpharm.2020.119148
43. Shiran MR, Akhtari J. Chitosan coating of anionic liposomes containing sumatriptan succinate: a candidate for nasal administration. *Nanomed J*. 2021;8(2). doi:10.22038/nmj.2021.08.002
44. Yu S, Xu X, Feng J, Liu M, Hu K. Chitosan and chitosan coating nanoparticles for the treatment of brain disease. *Int J Pharm*. 2019;560:282–293. doi:10.1016/j.ijpharm.2019.02.012
45. Aderibigbe BA, Naki T. Chitosan-based nanocarriers for nose to brain delivery. *Appl Sci*. 2019;9:11. doi:10.3390/app9112219
46. Sandri G, Motta S, Bonferoni MC, et al. Chitosan-coupled solid lipid nanoparticles: tuning nanostructure and mucoadhesion. *Eur J Pharm Biopharm*. 2017;110:13–18. doi:10.1016/j.ejpb.2016.10.010
47. Rigaut C, Deruyver L, Goole J, Haut B, Lambert P. Instillation of a dry powder in nasal casts: parameters influencing the olfactory deposition with uni- and bi-directional devices. *Front Med Technol*. 2022;4:1–17. doi:10.3389/fmedt.2022.924501
48. Manini G, Deldime M, Benali S, Raquez JM, Goole J. Long-acting implantable dosage forms containing paliperidone palmitate obtained by 3D printing. *Int J Pharm*. 2021;603:120702. doi:10.1016/j.ijpharm.2021.120702
49. Wong PT, Wang SH, Ciotti S, et al. Formulation and characterization of nanoemulsion intranasal adjuvants: effects of surfactant composition on mucoadhesion and immunogenicity. *Mol Pharm*. 2015;11(2):531–544. doi:10.1021/mp4005029.Formulation
50. Gonçalves VSS, Matias AA, Poejo J, Serra AT, Duarte CMM. Application of RPMI 2650 as a cell model to evaluate solid formulations for intranasal delivery of drugs. *Int J Pharm*. 2016;515(1–2):1–10. doi:10.1016/j.ijpharm.2016.09.086
51. Reichl S, Becker K. Cultivation of RPMI 2650 cells as an in-vitro model for human transmucosal nasal drug absorption studies: optimization of selected culture conditions. *J Pharm Pharmacol*. 2012;64(11):1621–1630. doi:10.1111/j.2042-7158.2012.01540.x
52. Wengst A, Reichl S. {RPMI} 2650 epithelial model and three-dimensional reconstructed human nasal mucosa as in vitro models for nasal permeation studies. *Eur J Pharm Biopharm*. 2010;74(2):290–297. doi:10.1016/j.ejpb.2009.08.008
53. Bai S, Yang T, Abbruscato TJ, Ahsan F. Evaluation of human nasal RPMI 2650 cells grown at an air–liquid interface as a model for nasal drug transport studies. *J Pharm Sci*. 2008;97(3):1165–1178. doi:10.1002/jps.21031
54. Gavini E, Rassu G, Ferraro L, et al. Influence of polymeric microcarriers on the in vivo intranasal uptake of an anti-migraine drug for brain targeting. *Eur J Pharm Biopharm*. 2013;83(2):174–183. doi:10.1016/j.ejpb.2012.10.010
55. Williams G, Suman JD. In vitro anatomical models for nasal drug delivery. *Pharmaceutics*. 2022;14(7):1353. doi:10.3390/pharmaceutics14071353
56. Charlton ST, Davis SS, Illum L. Evaluation of bioadhesive polymers as delivery systems for nose to brain delivery: in vitro characterisation studies. *J Control Release*. 2007;118:225–234. doi:10.1016/j.jconrel.2006.12.014
57. Scherließ R. Nasal formulations for drug administration and characterization of nasal preparations in drug delivery. *Ther Deliv*. 2020;11(3):183–191. doi:10.4155/tde-2019-0086
58. Mistry A, Stolnik S, Illum L. Nanoparticles for direct nose-to-brain delivery of drugs. *Int J Pharm*. 2009;379(1):146–157. doi:10.1016/j.ijpharm.2009.06.019
59. Shadab MD, Khan RA, Mustafa G, et al. Bromocriptine loaded chitosan nanoparticles intended for direct nose to brain delivery: pharmacodynamic, Pharmacokinetic and Scintigraphy study in mice model. *Eur J Pharm Sci*. 2013;48(3):393–405. doi:10.1016/j.ejps.2012.12.007
60. Rassu G, Soddu E, Cossu M, Gavini E, Giunchedi P, Dalpiaz A. Particulate formulations based on chitosan for nose-to-brain delivery of drugs. A review. *J Drug Deliv Sci Technol*. 2016;32:77–87. doi:10.1016/j.jddst.2015.05.002
61. Rassu G, Ferraro L, Pavan B, Giunchedi P, Gavini E, Dalpiaz A. The role of combined penetration enhancers in nasal microspheres on in vivo drug bioavailability. *Pharmaceutics*. 2018;10(4):8–10. doi:10.3390/pharmaceutics10040206
62. Raj R, Wairkar S, Sridhar V, Gaud R. Pramipexole dihydrochloride loaded chitosan nanoparticles for nose to brain delivery: development, characterization and in vivo anti-Parkinson activity. *Int J Biol Macromol*. 2018;109:27–35. doi:10.1016/j.ijbiomac.2017.12.056
63. von Halling Laier C, Sonne Alstrøm T, Travers Bargholz M, et al. Evaluation of the effects of spray drying parameters for producing cubosome powder precursors. *Eur J Pharm Biopharm*. 2019;135:44–48. doi:10.1016/j.ejpb.2018.12.008
64. Li L, Sun S, Parumasivam T, et al. L-Leucine as an excipient against moisture on in vitro aerosolization performances of highly hygroscopic spray-dried powders. *Eur J Pharm Biopharm*. 2016;102:132–141. doi:10.1016/j.ejpb.2016.02.010
65. Lechanteur A, Evrard B. Influence of composition and spray-drying process parameters on carrier-free DPI properties and behaviors in the lung: a review. *Pharmaceutics*. 2020;12:1. doi:10.3390/pharmaceutics12010055
66. Yue-Xing C, Fei-Fei Y, Han W, et al. The effect of L-leucine on the stabilization and inhalability of spray-dried solid lipid nanoparticles for pulmonary drug delivery. *J Drug Deliv Sci Technol*. 2018;46(151):474–481. doi:10.1016/j.jddst.2018.06.011
67. Cui Y, Zhang X, Wang W, et al. Moisture-resistant co-spray-dried netilmicin with l-leucine as dry powder inhalation for the treatment of respiratory infections. *Pharmaceutics*. 2018;10(4). doi:10.3390/pharmaceutics10040252
68. Chan JGY, Tyne AS, Pang A, et al. A rifapentine-containing inhaled triple antibiotic formulation for rapid treatment of tubercular infection. *Pharm Res*. 2014;31(5):1239–1253. doi:10.1007/s11095-013-1245-7
69. Chang YX, Yang JJ, Le PR, Chang Q, Liao YH. Anti-hygroscopic effect of leucine on spray-dried herbal extract powders. *Powder Technol*. 2014;266:388–395. doi:10.1016/j.powtec.2014.06.058
70. Aquino RP, Prota L, Auriemma G, et al. Dry powder inhalers of gentamicin and leucine: formulation parameters, aerosol performance and in vitro toxicity on CuFi1 cells. *Int J Pharm*. 2012;426(1–2):100–107. doi:10.1016/j.ijpharm.2012.01.026
71. Raula J, Thielmann F, Kansikas J, et al. Investigations on the humidity-induced transformations of salbutamol sulphate particles coated with L-leucine. *Pharm Res*. 2008;25(10):2250–2261. doi:10.1007/s11095-008-9613-4
72. Boraey MA, Hoe S, Sharif H, Miller DP, Lechuga-Ballesteros D, Vehring R. Improvement of the dispersibility of spray-dried budesonide powders using leucine in an ethanol-water cosolvent system. *Powder Technol*. 2013;236:171–178. doi:10.1016/j.powtec.2012.02.047

73. Wang X, Wan W, Lu J, Quan G, Pan X, Liu P. Effects of L-leucine on the properties of spray-dried swellable microparticles with wrinkled surfaces for inhalation therapy of pulmonary fibrosis. *Int J Pharm*. 2021;610:121223. doi:10.1016/j.ijpharm.2021.121223
74. Yarragudi SB, Kumar H, Jain R, Tawhai M, Rizwan S. Olfactory targeting of microparticles through inhalation and bi-directional airflow: effect of particle size and nasal anatomy. *J Aerosol Med Pulm Drug Deliv*. 2020;33(5):258–270. doi:10.1089/jamp.2019.1549
75. Schroeter JD, Tewksbury EW, Wong BA, Kimbell JS. Experimental measurements and computational predictions of regional particle deposition in a sectional nasal model. *J Aerosol Med Pulm Drug Deliv*. 2015;28(1):20–29. doi:10.1089/jamp.2013.1084
76. Shi H, Kleinstreuer C, Zhang Z. Modeling of inertial particle transport and deposition in human nasal cavities with wall roughness. *J Aerosol Sci*. 2007;38(4):398–419. doi:10.1016/j.jaerosci.2007.02.002
77. EMA. Invega, INN-paliperidone - scientific discussion; 2017.
78. Barriga HMG, Ces O, Law RV, Seddon JM, Brooks NJ. Engineering swollen cubosomes using cholesterol and anionic lipids. *Langmuir*. 2019;35(50):16521–16527. doi:10.1021/acs.langmuir.9b02336
79. Zabara A, Chong JTY, Martiel I, et al. Design of ultra-swollen lipidic mesophases for the crystallization of membrane proteins with large extracellular domains. *Nat Commun*. 2018;9:1. doi:10.1038/s41467-018-02996-5
80. Sou T, McIntosh MP, Kaminskas LM, Prankerd RJ, Morton DAV. Designing a multicomponent spray-dried formulation platform for pulmonary delivery of biomacromolecules: the effect of polymers on the formation of an amorphous matrix for glassy state stabilization of biomacromolecules. *Dry Technol*. 2013;31(13–14):1451–1458. doi:10.1080/07373937.2013.788019
81. Gates-Rector S, Blanton T. The powder diffraction file: a quality materials characterization database. *Powder Diffr*. 2019;34(4):352–360. doi:10.1017/S0885715619000812
82. Nasr M, Ghorab MK, Abdelazem A. In vitro and in vivo evaluation of cubosomes containing 5-fluorouracil for liver targeting. *Acta Pharm Sin B*. 2015;5(1):79–88. doi:10.1016/j.apsb.2014.12.001
83. Mangal S, Meiser F, Tan G, et al. Relationship between surface concentration of l-leucine and bulk powder properties in spray dried formulations. *Eur J Pharm Biopharm*. 2015;94:160–169. doi:10.1016/j.ejpb.2015.04.035
84. Foo MY, Cheng Y-S-S, Su W-C-C, Donovan MD. The influence of spray properties on intranasal deposition. *J Aerosol Med*. 2007;20 (4):495–508. doi:10.1089/jam.2007.0638
85. Moraga-Espinoza D, Warnken Z, Moore A, Williams RO, Smyth HDCC. A modified USP induction port to characterize nasal spray plume geometry and predict turbinate deposition under flow. *Int J Pharm*. 2018;548(1):305–313. doi:10.1016/j.ijpharm.2018.06.058
86. Pu Y, Goodey AP, Fang X, Jacob K. A comparison of the deposition patterns of different nasal spray formulations using a nasal cast. *Aerosol Sci Technol*. 2014;48(9):930–938. doi:10.1080/02786826.2014.931566
87. Van Strien J, Petersen P, Lappas P, et al. Spray characteristics from nasal spray atomization. *J Aerosol Sci*. 2022;165. doi:10.1016/j.jaerosci.2022.106009
88. Inthavong K, Tian ZF, Tu JY, Yang W, Xue C. Optimising nasal spray parameters for efficient drug delivery using computational fluid dynamics. *Comput Biol Med*. 2008;38(6):713–726. doi:10.1016/j.compbiomed.2008.03.008
89. Kaliner M, Shelhamer JH, Borson B, et al. Human respiratory mucus. *J Allergy Clin Immunol*. 1984;73(3):318–323. doi:10.1016/0091-6749(84)90403-2
90. Nikogeorgos N, Efler P, Kayitmazer AB, Lee S. "Bio-glues" to enhance slipperiness of mucins: improved lubricity and wear resistance of porcine gastric mucin (PGM) layers assisted by mucoadhesion with chitosan. *Soft Matter*. 2015;11(3):489–498. doi:10.1039/c4sm02021a
91. Yakubov GE, Papagiannopoulos A, Rat E, Waigh TA. Charge and interfacial behavior of short side-chain heavily glycosylated porcine stomach mucin. *Biomacromolecules*. 2007;8(12):3791–3799. doi:10.1021/bm700721c
92. Bansil R, Turner BS. The biology of mucus: composition, synthesis and organization. *Adv Drug Deliv Rev*. 2018;124:3–15. doi:10.1016/j.addr.2017.09.023
93. Sogias IA, Williams AC, Khutoryanskiy VV. Why is chitosan mucoadhesive? *Biomacromolecules*. 2008;9(7):1837–1842. doi:10.1021/bm800276d
94. Mazzarino L, Travelet C, Ortega-Murillo S, et al. Elaboration of chitosan-coated nanoparticles loaded with curcumin for mucoadhesive applications. *J Colloid Interface Sci*. 2012;370(1):58–66. doi:10.1016/j.jcis.2011.12.063
95. Pardeshi CV, Belgamwar VS. Direct nose to brain drug delivery via integrated nerve pathways bypassing the blood–brain barrier: an excellent platform for brain targeting. *Expert Opin Drug Deliv*. 2013;10(7):957–972. doi:10.1517/17425247.2013.790887
96. Djupesland PG. Nasal drug delivery devices: characteristics and performance in a clinical perspective—a review. *Drug Deliv Transl Res*. 2013;3 (1):42–62. doi:10.1007/s13346-012-0108-9
97. Nakamura H, Watano S. Direct permeation of nanoparticles across cell membrane: a review. *KONA Powder Part J*. 2018;2018(35):49–65. doi:10.14356/kona.2018011
98. Salatin S, Maleki Dizaj S, Yari Khosroushahi A. Effect of the surface modification, size, and shape on cellular uptake of nanoparticles. *Cell Biol Int*. 2015;39(8):881–890. doi:10.1002/cbin.10459
99. Arvizo RR, Miranda OR, Thompson MA, et al. Effect of nanoparticle surface charge at the plasma membrane and beyond. *Nano Lett*. 2010;10 (7):2543–2548. doi:10.1021/nl101140t
100. Clementino AR, Pellegrini G, Banella S, et al. Structure and fate of nanoparticles designed for the nasal delivery of poorly soluble drugs. *Mol Pharm*. 2021;18(8):3132–3146. doi:10.1021/acs.molpharmaceut.1c00366
101. Albarki MA, Donovan MD. Uptake of cationic PAMAM-PLGA nanoparticles by the nasal mucosa; 2022.
102. Akilo OD, Choonara YE, Strydom AM, et al. AN in vitro evaluation of a carmustine-loaded Nano-co-Plex for potential magnetic-targeted intranasal delivery to the brain. *Int J Pharm*. 2016;500(1–2):196–209. doi:10.1016/j.ijpharm.2016.01.043
103. Fröhlich E. The role of surface charge in cellular uptake and cytotoxicity of medical nanoparticles. *Int J Nanomed*. 2012;7:5577–5591. doi:10.2147/IJN.S36111